Full Paper

Propellants, Explosives, Pyrotechnics

DOI: 10.1002/prep.201800390

Comparative Analysis of Detonation Growth Characteristics between HMX- and TATB-based PBXs

Zhiling Bai,[a] Zhuoping Duan,*[a] Lijing Wen,[b] Zhenyu Zhang,[c] Zhuocheng Ou,[a] and Fenglei Huang[a]

Abstract: This paper offers a new method for calculating the reaction rate based on the pore collapse "hot-spot" ignition mechanism in multi-component polymer bonded explosives (PBXs), and proposes a mesoscopic reaction rate model that allows us to predict the shock initiation and detonation behaviors of multi-component PBXs with any explosive component proportion and explosive particle size. The pressure-time histories in PBXC03 (87% HMX, 7% TATB, and 6% Viton by weight) and PBXC10 (25% HMX, 70% TATB, and 5% Kel-F800 by weight) are calculated by using the new mesoscopic reaction rate model, and the numerical results are found to be in good agreement with the experimental data. It is found that the shock initiation and detonation behaviors of PBXC03 with the dominant component of HMX is mainly controlled by the hot-spot ignition. The subsequent combustion reacts fast once the hot-spot is ignited and shows an accelerated reaction characteristic. While, with the dominant component of insensitive TATB, the critical initiation pressure of PBXC10 is high enough to make almost saturated reactive hot spots just behind the precursory shock-wave front, and the shock initiation behavior is basically determined by the combustion reaction, which is characterized by a stable reaction due to the slow combustion-wave velocity.

Keywords: shock initiation · multi-component PBX explosives · mesoscopic reaction rate model · reaction rate-time history

1 Introduction

HMX (octahydro-1,3,5,7-tetranitro-1,3,5,7-tetrazine) has been subjected to extensive research during the past few decades for its high energy performance, while it is sensitive to external stimuli (e.g., high temperature, impact and friction) [1–3]. TATB (1,3,5-triamino-2,4,6-trinitrobenzene) belongs to the high thermal stabilized and insensitive high explosives, but it exhibits lower released energy [4–6]. Therefore, to satisfy the requirements of high performance and low sensitivity, mixing HMX and TATB at a certain ratio to prepare a HMX/TATB-based polymer bonded explosive (PBX), such as the commonly used PBXC03 (87% HMX, 7% TATB, and 6% Viton by weight) [7,8] and the insensitive PBXC10 (25% HMX, 70% TATB, and 5% Kel-F800 by weight) [7,9], is an effective method to balance the contradiction between energy release and sensitivity [10,11] and a direction for the formulation design of multi-component explosives. Moreover, it is well known that the detonation growth behaviors and the energy release characteristics of the HMX component is very much different from that of the TATB component, depending on each of their own reaction mechanism. Recently, K. F. Grebenkin [12] proposed a three-factors model (i.e., the density of the reactive hot spots, the velocity of the combustion wave and the combustion geometric topology), and pointed out that the lower shock sensitivity of the TATB-based PBX explosive is resulted from the low temperature of its detonation products and the macroscopic chemical reaction in HMX is determined by the density of hot spots, whereas the macrokinetics in TATB is basically determined by the propagating velocity of the combustion waves coming from the hot spots. That is to say, the detonation performance of a HMX/TATB-based PBX explosive depends on both the component contents and the mesostructure (such as the particle size and the porosity).

For a PBX explosive, one kind of typical heterogeneous solid explosives, the pore collapse that including the viscoplastic deformation, the hydrodynamic micro-jetting, the compression of gas in cavities and the shear bandings is a dominant mechanism of "hot-spot" formation during the shock initiation process [13,14], and the explosive maybe enter the detonation growth process once the "hot-spot" is ignited, which is mainly described by the surface combustion mechanism [15,16]. Generally, the reactive hot spots in PBX have the temporal and spatial scales on the order of nanosecond and micron, respectively [17,18], and it is suggested that the shock intensity, the material viscosity, and the initial pore's size and shape all have noticeable effect

[a] *Z. Bai, Z. Duan, Z. Ou, F. Huang*
The State Key Laboratory of Explosion Science and Technology, Beijing Institute of Technology, Beijing 100081, P.R. China
**e-mail: duanzp@bit.edu.cn*
[b] *L. Wen*
Nuclear and Radiation Safety Center, Ministry of Environmental Protection, Beijing 100082, P.R. China
[c] *Z. Zhang*
Institute of Technical Physics, College of Science, National University of Defense Technology, Changsha 410073, P.R. China

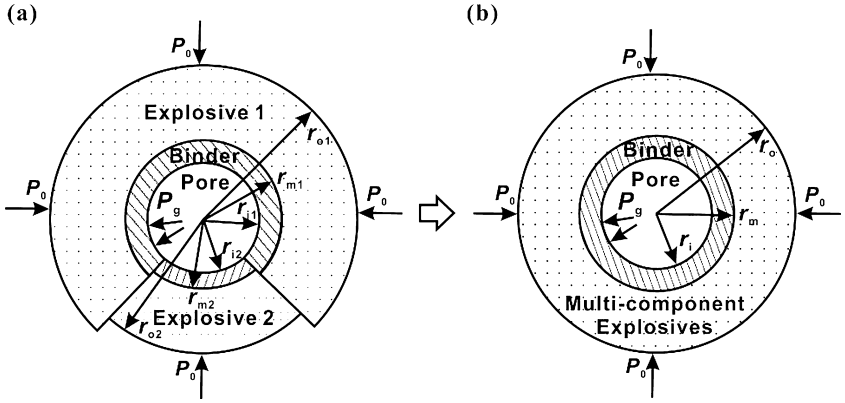

Figure 1. Illustration of the simplification from an irregular double-layers hollow sphere model to a spherically symmetric double-layers hollow sphere model for a two-component PBX explosive.

on the hot-spot formation [19–24]. To quantitatively describe the reactive flow field of the shock initiation and detonation processes in heterogeneous solid explosives, a number of reaction rate models have been proposed over the years, included mainly the empirical macroscopic models [25–28], the statistical models [29–31] and the mesoscopic models [14, 15, 32, 33]. However, these models show lower precision for quantitatively evaluating the influence of both the explosive's component-content and mesostructure on the shock ignition and detonation characteristics of multi-component explosives.

In this paper, based on the multiple spherical pore collapse hot-spot mechanism [33], a new multi-component mesoscopic reaction rate model for the multi-component PBXs is developed. Based on the previous experimental data, the numerical simulations are performed on both PBXC03 and PBXC10 (both having the same explosive components but in different proportions) with different explosive particle sizes to investigate the influence of both the explosive component-content and the particle size on the shock initiation and detonation behaviors and verify the applicability of the new chemical reaction rate model. Moreover, on both the chemical reaction degree and the reaction rate histories are also focused for deeply understanding the reactive flow field information.

2 The New Multi-component DZK Reaction Rate Model

The multi-component DZK reaction rate model proposed by Liu et al. [33] is:

$$\frac{\mathrm{d}\lambda(x,t)}{\mathrm{d}t} = \frac{\mathrm{d}\lambda_h}{\mathrm{d}t} + 3\sum_{l=1}^{j}\chi_l\frac{\lambda_l^{2/3}}{r_{ol}}a_l p^{n_l} + \sum_{l=1}^{j}\chi_l G_l p^{m_l}(1-\lambda)^{s_l} \quad (1)$$

where the subscript "h" denotes the hot-spot ignition contribution, and $\lambda(x, t)$ is the overall chemical reaction degree (the volume fraction of the reacted explosive) at the Euler location x and time t; p is the current pressure (Mbar); λ_l, χ_l, r_{ol} are the reaction degree, the volume fraction and the average radius of the l-th explosive component ($l = 1, 2, \ldots, j$), respectively. Moreover, a_l, n_l, G_l, m_l, and s_l are constant coefficients for the l-th explosive component. In addition, the first term on the right-hand side of Eq. (1) describes the hot-spot forming phase, and the last two terms describe the slow burning at the low-pressure stage and the fast overall reaction at the high-pressure phase for multi-component explosives, respectively. Compared with the DZK reaction rate model for a single-component explosive [32], the last two terms in Eq. (1) are equal to the linear addition of that of each explosive component weighted by the volume ratio at each stage, respectively. Moreover, an irregular double-layers hollow sphere is used to describe the hot-spot formation resulted from the pore collapse mechanism in multi-component PBX explosives, see Figure 1 (a) for a two-component PBX explosive as an example. The outer radius r_{ol} and the inner radius r_{il} are the mean radii of the l-th explosive component particles and the pore, respectively; r_{ml} is the radius of the interface between the binder and the l-th explosive component. P_0 and P_g are the shock-wave pressure on the outer surface of the explosive sphere and the gas pressure inside the pore, respectively.

To overcome the difficulty in solving the complicated initial-boundary value problem of an elastic/viscoplastic irregular double-layers hollow sphere collapse, a "mixing rule" of the explosive components was introduced by Liu et al. [33] to obtain a set of equivalent thermodynamic parameters for the multi-component explosives by weighted average of all explosive components. Moreover, the irregular double-layers hollow sphere model was simplified to a spherically symmetric double-layers hollow sphere model (see Figure 1 (b)), and then the hot-spot ignition term in Eq. (1) was obtained.

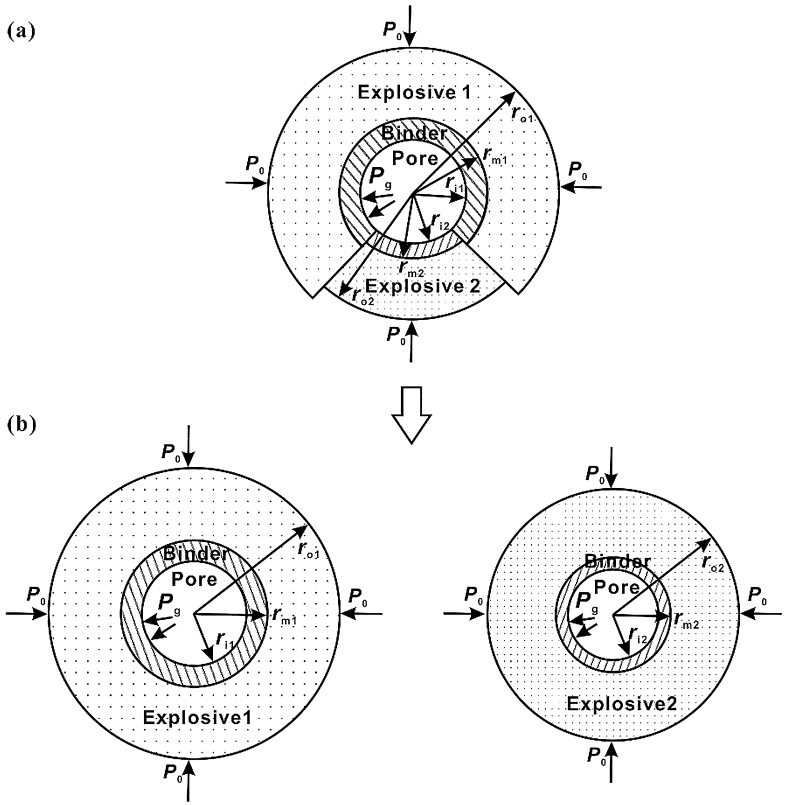

Figure 2. Illustration of dividing the original irregular double-layers hollow sphere model into two spherically symmetric double-layers hollow sphere models for a two-componet PBX explosive.

In the opinion of the present authors, after the above simplification, although this multi-component DZK reaction rate model can be used to describe the effect of the explosive component content on shock ignition and the detonation growth processes of the multi-component PBX explosives, it fails to estimate the influence of the mesostructure. In fact, for example, the particle size of the explosive is a very important geometric parameter, if HMX and TATB with considerably different particle sizes are "mixed" into an equivalent double-layers hollow sphere, the influence of each explosive component's particle size will be drowned out.

For this reason, a new method to deal with the pore collapse forming hot-spot model for multi-component PBX explosives is developed in this paper. For simplicity, the hydrodynamic interaction among each explosive component is neglected during the transient pore collapse process, which implies that each explosive component deforms independently. As is shown in Figure 2, the original elastic/viscoplastic irregular double-layers hollow sphere model is now divided into two independent elastic/viscoplastic spherically symmetric double-layers hollow sphere models, based on which, a new mesoscopic reaction rate model for shock initiation of multi-component PBXs can be established.

It should be pointed out here that, in fact, as the chemical reaction continues, the reacted gas products of all the explosive components fill into the pore and they are fully mixed quickly, which implies that the gas pressure P_g inside the pores are the same for each hollow sphere model. By using Dalton's law of partial pressure, there is

$$P_g = \sum_{l=1}^{j} \chi_l P_{gl} \tag{2}$$

where P_{gl} is the partial pressure of the gas product of the l-th explosive component.

The DZK reaction rate model for a single-component PBX explosive [32] is adopted here to calculate the reaction rate of each explosive component. Moreover, a burn-up factor $(1-\lambda_l)^{bl}$ is introduced in the low-pressure slow burning term for each explosive component, with b_l the constant coefficient. Finally, the reaction rate for multi-component PBX explosives are obtained by a linear superposition of all the explosive components, and then the new multi-component DZK reaction rate model for shock initiation of multi-component PBX explosives is reached as follows:

$$\frac{\mathrm{d}\lambda(x,t)}{\mathrm{d}t} = \sum_{l=1}^{j} \chi_l \left[\frac{\mathrm{d}\lambda_{hl}(x,t)}{\mathrm{d}t} + \frac{3\lambda_l^{2/3}(1-\lambda_l)^{b_l}}{r_{ol}} a_l p^{n_l} + G_l p^{m_l}(1-\lambda)^{s_l}\right] \tag{3}$$

where the trinomial in the square bracket is the chemical reaction rate of the *l*-th explosive component. The first term is the reaction rate of hot-spot ignition, in which the parameters are the thermodynamic parameters of the *l*-th explosive component; the constant parameters a_l, b_l, n_l, G_l, m_l, s_l in the last two combustion terms can be determined by fitting a typical experimental data of the *l*-th explosive component.

Moreover, the explosive's porosity α is defined as the ratio of the pore volume to the explosive volume, which can also be expressed as a function of the actual density ρ and the theoretical density ρ_T of the explosive as

$$\alpha = 1 - \frac{\rho}{\rho_T} = \frac{\sum_{l=1}^{j} N_l r_{il}^3}{\sum_{l=1}^{j} N_l r_{ol}^3} = \frac{\sum_{l=1}^{j} \chi_l \alpha_l}{\sum_{l=1}^{j} \chi_l} \tag{4}$$

where N_l, χ_l and α_l are the total particle number, the volume fraction and the porosity of the *l*-th explosive component, respectively. The binder content β is defined as the volume ratio of the binder to the explosive. That is

$$\beta = \frac{V_b}{V_e} = \frac{\sum_{l=1}^{j} N_l (r_{ml}^3 - r_{il}^3)}{\sum_{l=1}^{j} N_l (r_{ol}^3 - r_{ml}^3)} = \frac{\sum_{l=1}^{j} \chi_l \beta_l \frac{1-\alpha_l}{1+\beta_l}}{\sum_{l=1}^{j} \chi_l \frac{1-\alpha_l}{1+\beta_l}} \tag{5}$$

where V_b and V_e are the total volumes of the binder and the explosive components, respectively. β_l is the volume ratio of the binder to the *l*-th explosives component in the double-layers hollow sphere model.

In general, it is almost impossible to distinguish both porosities and binder contents of different explosives components during the PBXs synthesis. To determine practically the values of α_l and β_l, for simplicity, it is assumed that all the explosive components have the same porosity, namely,

$$\alpha_l = \frac{r_{il}^3}{r_{ol}^3} \equiv \alpha (l = 1, \cdots, j) \tag{6}$$

and all the binder contents β_l ($l = 1, 2, \ldots j$) are assumed to take the same value β, i.e.,

$$\beta_l = \frac{r_{ml}^3 - r_{il}^3}{r_{ol}^3 - r_{ml}^3} \equiv \beta (l = 1, \cdots, j) \tag{7}$$

From the point view of statistical average, to some extent, the above simplified operation is generally accepted in practical applications. Thus, for a given explosive, r_{ml} can be solved from Eq. (6) and Eq. (7) with the known r_{ol}, α, and β.

The HMX/TATB-based explosives PBXC03 and PBXC10 can be considered as multi-component explosives composed of HMX-based PBX explosive PBX9501 (95 % HMX, 2.5 % Estane, and 2.5 % BDNPA/BDNPF by weight) and TATB-based PBX explosive LX-17 (92.5 %TATB, 7.5 %Kel-F800 by weight), in which HMX/TATB are original components and PBX9501/LX-17 are the so-called substituted components. The calculated volume fractions of these two substituted components in PBXC03 and PBXC10 are shown in Table 1.

The values of the parameters in the first hot-spot ignition term for the components HMX and TATB are given in Table 2 [33, 34], and Table 3 shows the values of the parameters in the last two combustion terms, which are de-

Table 1. Volume fractions of each substituted explosive component in PBXC03 and PBXC10.

Parameters	PBX9501 (HMX-based)	PBXC03	PBXC10	LX-17 (TATB-based)
χ_1	1	0.923193	0.247764	0
χ_2	0	0.076807	0.752236	1

Table 2. Thermodynamic parameters of the hot-spot ignition term for the HMX and the TATB [33, 34].

Parameters	HMX	TATB
Heat of Reaction (Q) ($cm^2/\mu s^2$)	5.439e−2	2.510e−2
Heat capacity (C_p) ($cm^2/\mu s^2/K$)	1.4e−5	2.005e−5
Frequency factor (Z) (μs^{-1})	5.0e+13	3.18e+13
Activation temperature (T^*) (K)	26500	30140.8
Initial temperature (T_0) (K)	298	298
Thermal conductivity (k^*) (cm/μs/K)	8.0e−14	1.14e−13
Shear yield strength (k_e) (Mbar)	8.0e−5	8.0e−5
Constant related to viscosity (γ_e) (μs^{-1})	0.026	0.026

Table 3. Parameters of the second and the third terms in Eq. (3) for PBX9501 and LX-17.

Parameters l=1,2	PBX9501 (HMX-based)	LX-17 (TATB-based)
a_l	0.027	0.01
b_l	2.05	1.70
n_l	1.00	2.03
G_l	800.0	220.0
m_l	3.355	3.077
s_l	1.00	0.2

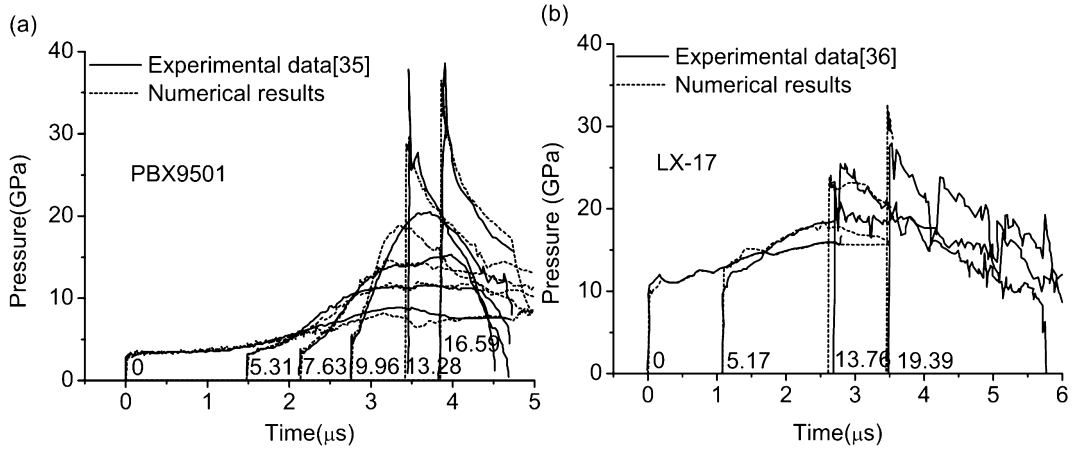

Figure 3. Experimental data and Numerical results for the pressure-time histories in the HMX-based PBX9501 and the TATB-based LX-17: (a) PBX9501, (b) LX-17.

termined by fitting the shock initiation experimental data of the PBX9501 [35] and the LX-17 [36], respectively. The numerical results for the pressure-time histories at different Lagrangian locations in the PBX9501 and the LX-17, together with the corresponding experimental data are shown in Figure 3. It can be seen that the numerical results are all in good agreement with the experimental data. The values of the parameters listed in Table 2 and Table 3 are used in all the following numerical simulations in section 3 and section 4.

3 Numerical Simulation and Results

Recently, Wen et al. [7] have performed a series of shock initiation experiments on PBXC03 and PBXC10 to obtain in-situ pressure gauge data, in which the shock-wave loading was obtained by using an explosive plane-wave lens, and both the component proportions and the physical parameters of the used explosive samples [9] are listed in Table 4. In this paper, the new multi-components DZK reaction rate model is incorporated into a DYNA2D code to simulate numerically the shock ignition and the detonation growth processes of the PBXC03 and the PBXC10 explosives, respectively. In all the simulations, the experimentally measured pressure-time curves at the 0 mm gauge depth are taken as the loading boundary conditions. What's more, the Jones-Wilkins-Lee (JWL) equations of state (EOS) in the form of temperature dependence are adopted for both the detonation products and the un-reacted explosives, and the values of the parameters in JWL EOS [33] are listed in Table 5.

In addition, the manganin gauges and the Teflon films were embedded in the experimental explosive samples, which have also taken into account in the modeling, and their parameter values in the Grüneisen equations of state are listed in Table 6 [35].

Table 5. Parameters in JWL EOS for detonation products and un-reacted PBXC03 and PBXC10 [33].

Parameters	PBXC03 Products	Un-reacted	PBXC10 Products	Un-reacted
A (Mbar)	10.2545	272137.59	6.128	127.34089
B (Mbar)	0.2257	−0.738544	0.1858	−0.089820
R_1	4.91	19.87	4.32	10.4
R_2	1.37	1.987	1.79	1.04
ω	0.29	1.99	0.21	2.50
C_v (Mbar/K)	1.0e−5	1.6932e−4	1.0e−5	3.73122e−5
E_0 (Mbar)	0.1	–	0.1	–

The numerical results for pressure-time histories of PBXC03 and PBXC10 with different explosive particle sizes as well as the experimental data are shown in Figure 4 and

Table 4. Components and physical parameters of PBXC03 and PBXC10 [7].

Explosives	Components proportion HMX/TATB/Binder		Density ρ (g/cm^3)	Theoretical density ρ_T (g/cm^3)	Mean particle size(μm)	
	Weight (%)	Volume (%)			HMX	TATB
PBXC03	87/7/6	85.58/6.76/7.66	1.849	1.873	20–30 (fine particle)	15
PBXC10	25/70/5	25.4/69.8/4.8	1.900	1.934	70–90 (medium particle) 100–130 (coarse particle)	

Table 6. Parameters in the Grüneisen EOS for the manganin and the teflon [35].

Materials	ρ_0 (g/cm^3)	C(cm/μs)	S_1	S_2	S_3	γ_0	a
Manganin	8.14	0.394	1.489	0	0	2.02	0.47
Teflon	2.15	0.168	1.123	3.983	−5.797	0.59	0

Figure 5, respectively. It can be seen that the numerical results are all in good agreement with the experimental data, which indicates that the new multi-component DZK reaction rate model can preferably predict the influence of both the explosive component proportion and the explosive particle size on the shock initiation processes of multi-component PBX explosives. It is worth mentioning that the shock initiation response of heterogeneous solid explosives is actually the result of the interaction of multiple hot spots with variant sizes and shapes. However, the present model is a statistical average operation, the errors on the pressure growth and peaks are probably caused mainly by the inaccuracy of the model.

The experimental data and the numerical results for the precursory shock-wave trajectories in PBXC03 and PBXC10 with different particle sizes are shown in Figure 6. It can be seen that there is satisfactory coincident with the calculated arrival time of the shock wave and that of the experimental data. The uncertainty of the numerical results is mainly from the pressure growth and the peak pressure. Moreover, it can be observed that the smaller the explosive particle size, the shorter the run distance to detonation, which is consistent with the general conclusions in previous works [37–39].

In addition, Li et al. [40] conducted the shock initiation experiments on both PBXC03 and PBXC10 to gain insight into the reaction mechanisms for the shock initiation and detonation processes, in which an aluminum flyer driven by the gun was used to impact the explosive samples. In this section, the corresponding numerical simulations are carried out for further verification of the new multi-component DZK model. As is shown in Figure 7, the calculated results are in good agreement with the experimental data, which indicates again that the new reaction rate model can be

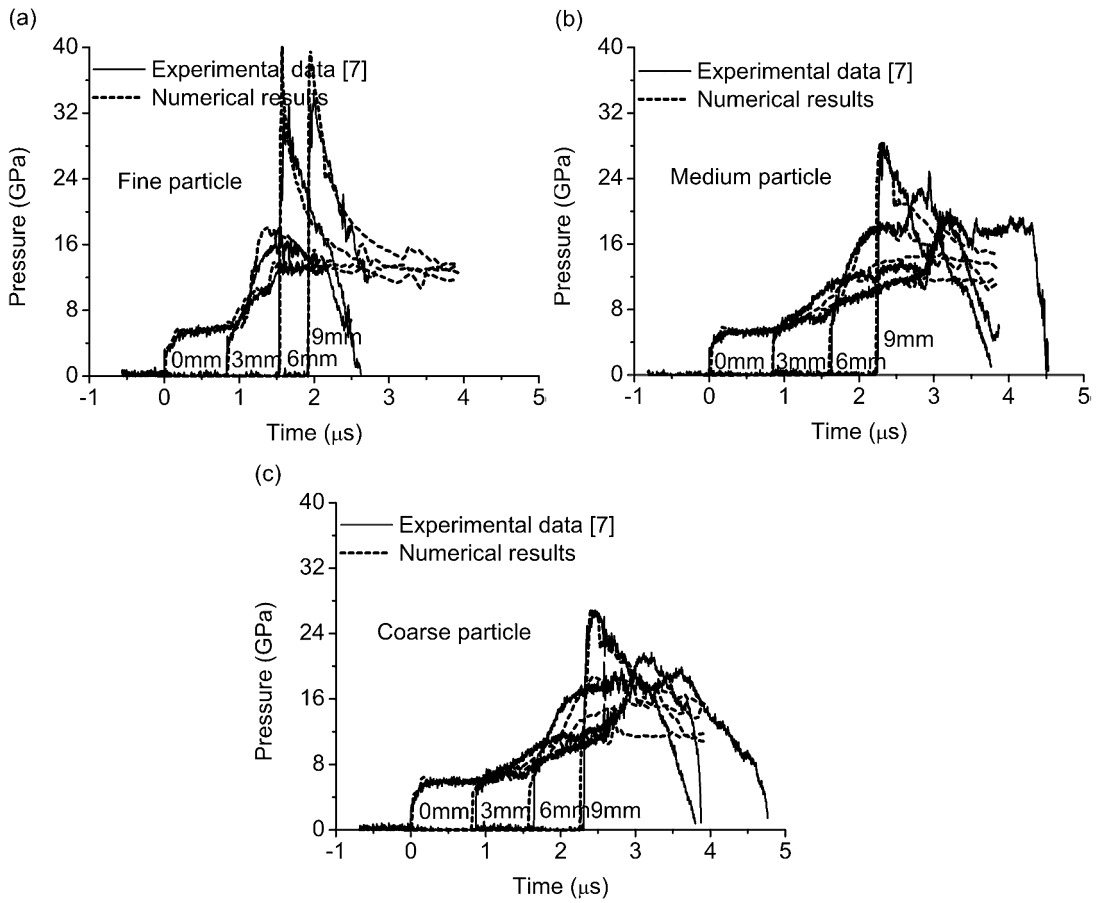

Figure 4. Experimental data and numerical results for the pressure-time histories in PBXC03 with different particle sizes: (a) the fine particle; (b) the medium particle; and (c) the coarse particle.

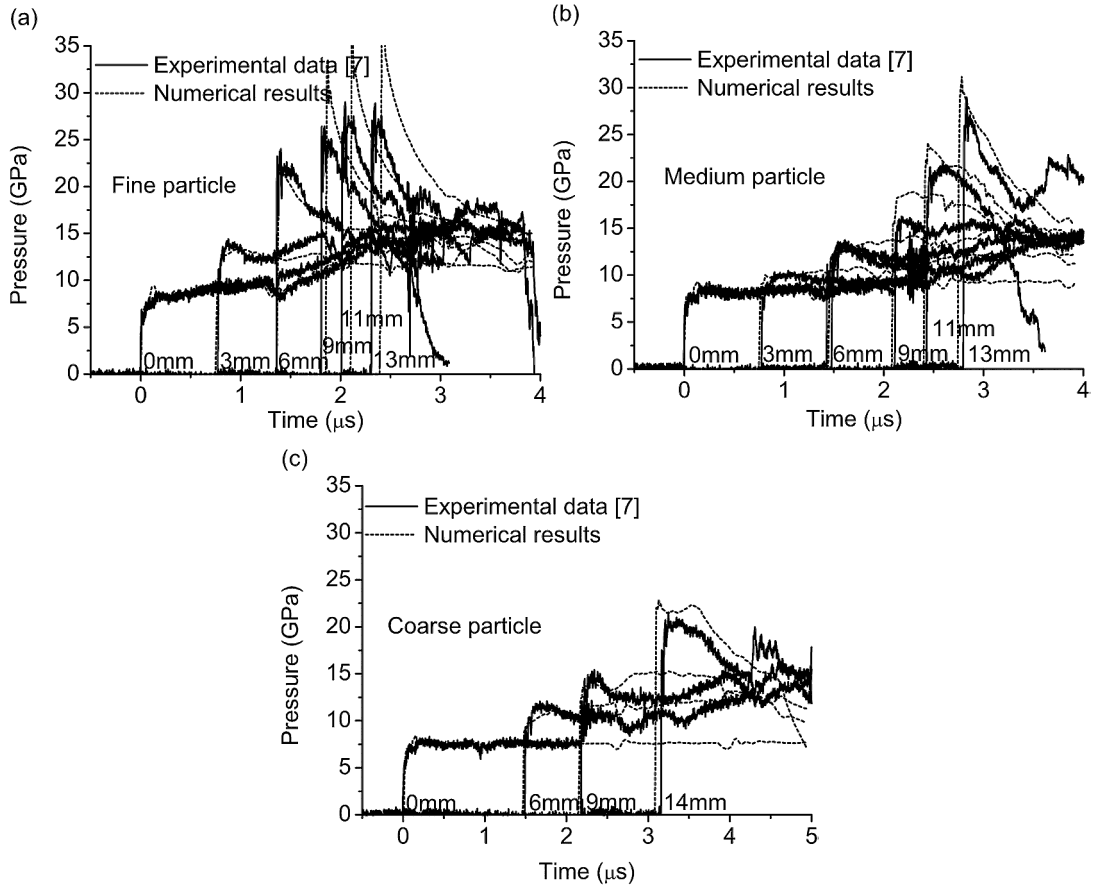

Figure 5. Experimental data and numerical results for the pressure-time histories in PBXC10 with different particle sizes: (a) the fine particle; (b) the medium particle; and (c) the coarse particle.

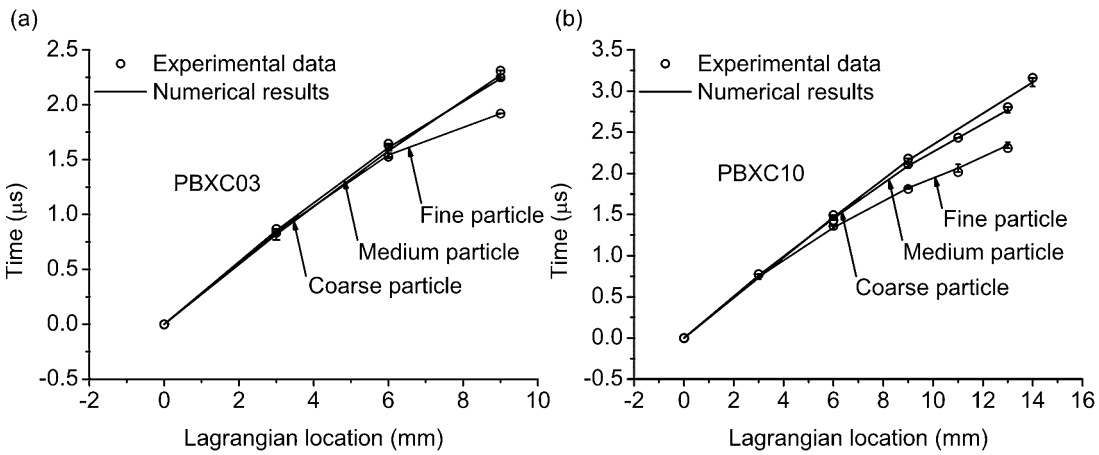

Figure 6. Experimental data and numerical results for the precursory shock-wave trajectories in PBXC03 and PBXC10 with different particle sizes: (a) PBXC03; (b) PBXC10.

adopted to predict the shock initiation process of the HMX/TATB-based PBXs under different loading conditions.

It is also found that the shock ignition and detonation growth processes of PBXC03 is distinctly different from that of PBXC10. For example, the pressure-time histories of PBXC03 are in a shape of hump that the pressure on the precursory shock-wave front increases slowly, but the pressure behind the shock wave grows faster and keeps in chas-

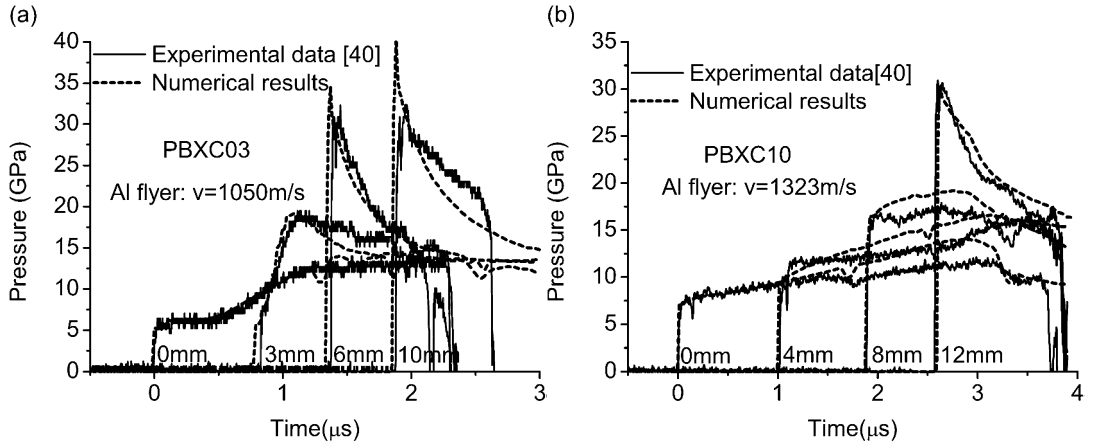

Figure 7. Experimental data and numerical results for the pressure-time histories for PBXC03 and PBXC10 impacted by an aluminum flyer: (a) PBXC03, (b) PBXC10.

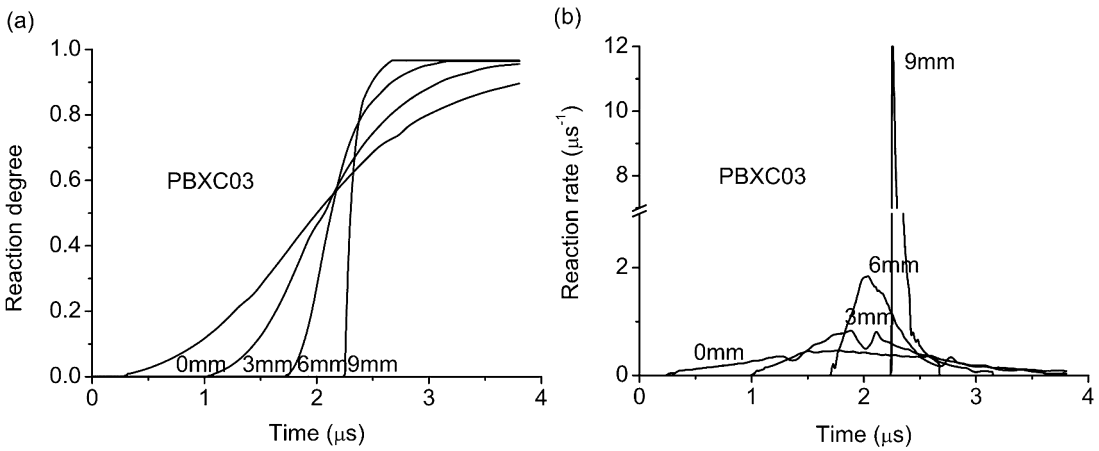

Figure 8. Typical reaction degree-time histories and reaction rate-time histories at different Lagrange locations in PBXC03.

ing the precursory shock wave until a full detonation is formed. On the contrary, in PBXC10, the pressure-time histories show as a shape of step increase. That is to say, the increase of the pressure on the precursory shock-wave front is relatively large, while the pressure behind the shock wave almost has no any obvious growth, which indicates that the physical mechanisms of the shock initiation and the detonation growth of the HMX-based PBXs is different from that of the TATB-based PBXs.

Additionally, it is worth pointing out here that the parameters in the new multi-component DZK reaction rate model can be obtained directly from that of the DZK reaction rate model for each explosive component, with no re-calibration for the parameter of multi-component PBXs with any explosive component proportion needed.

4 Physical Mechanisms Analysis

To understand more well the physical mechanisms of the shock initiation and the detonation growth processes in the HMX-based and the TATB-based PBXs, the new multi-component DZK reaction rate model is also used to obtain the time histories of some other physical variable in the reactive flow field.

The typical time histories of the chemical reaction degree and the chemical reaction rate at different Lagrangian locations in PBXC03 and PBXC10 are shown in Figure 8 and Figure 9, respectively. It is found in PBXC03, that the reaction rate is small just behind the precursory shock-wave front and the peak value appears quite a time after the shock wave passed. The reason is that the critical initiation pressure of PBXC03 with the dominant explosive component HMX is lower, so that there are relatively fewer reactive hot spots and the hot-spot ignition reaction is slower just behind the precursory shock-wave front. With the

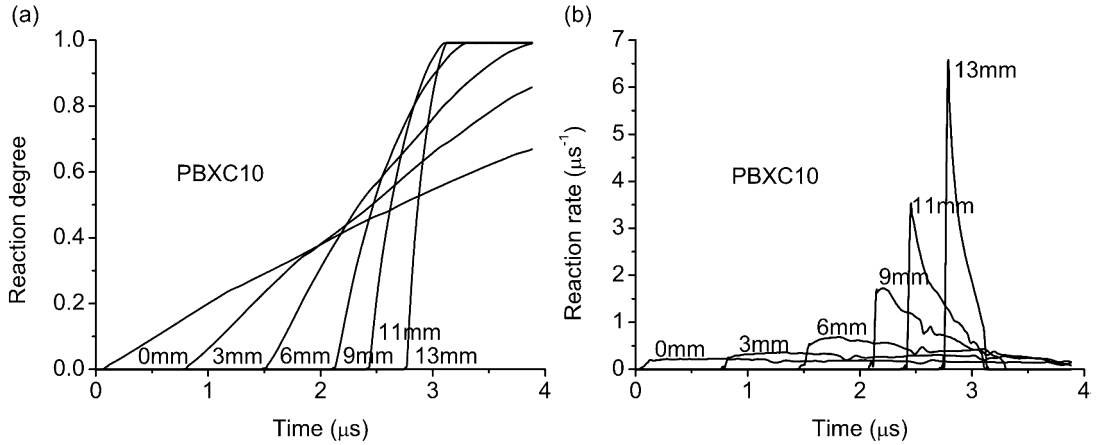

Figure 9. Typical reaction degree-time histories and reaction rate-time histories at different Lagrange locations in PBXC10.

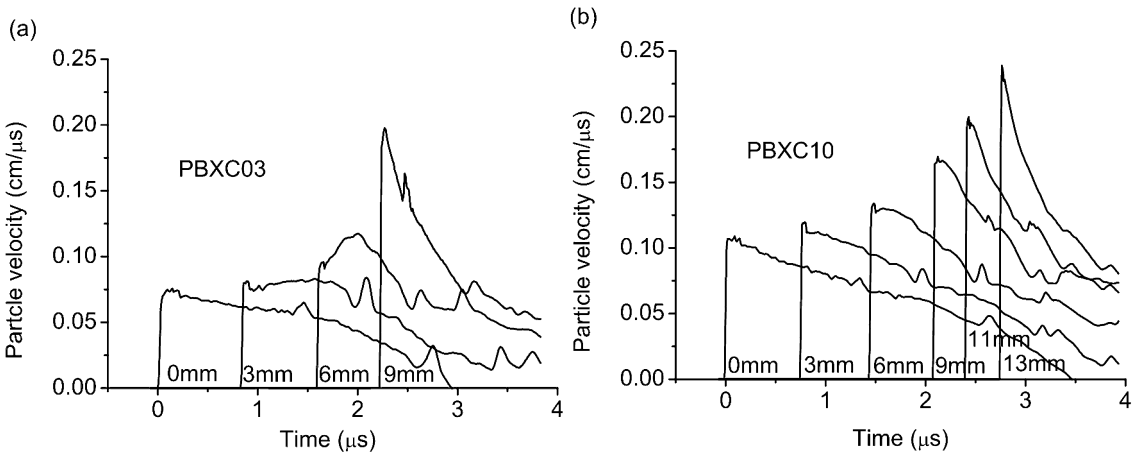

Figure 10. Typical particle velocity-time histories at different Lagrange locations in PBXC03 and PBXC10.

chemical reaction goes on, more reactive hot spots are generated by the compression wave, and the combustion reacts faster, which causes the increase of the pressure behind the precursory shock-wave front. The accelerated reaction characteristics of HMX-based PBXC03 is consistent with the general process of shock initiation to detonation in heterogeneous high explosives, during which the shock acceleration results directly from the local reaction, and the strengthened shock then produces an increasing number of igniting hot spots. A large number of small pressure waves propagate from these sites, coalescing into a large pressure disturbance which overtakes and progressively amplifies the shock until detonation is reached. However, in PBXC10, the peak reaction rate occurs near the precursory shock-wave front, because that the critical initiation pressure of PBXC10 with the main explosive component TATB is high, there are almost saturated reactive hot-spots and the chemical reaction is extremely fast just behind the initial shock-wave front, which means that the density of hot spots can be considered as a constant in modeling the shock initiation to detonation process. On the other hand, the temperature of the gas products of TATB is low (about half of those of HMX [12]), which causes the slow combustion reaction behind the precursory shock-wave front featured by a stable reaction characteristic. In addition, it is worth mentioning that, comparing with the homogeneous reaction mechanisms, a basically different view is that the energy release due to local thermal explosions is relatively small, the large pressure disturbances are generated by the sustained burning around hot-spot sites.

Moreover, the typical time histories of the particle velocity at different Lagrangian locations in PBXC03 and PBXC10 are shown in Figure 10, respectively. It can be seen that the peak particle velocity in PBXC03 appears a certain period of time behind the precursory shock-wave front, while in PBXC10, the peak particle velocity occurs almost just behind the precursory shock-wave front.

Furthermore, Figure 11 shows the trajectories of the precursory shock-wave front, the peak particle velocity, the peak reaction rate and the peak pressure in PBXC03 and

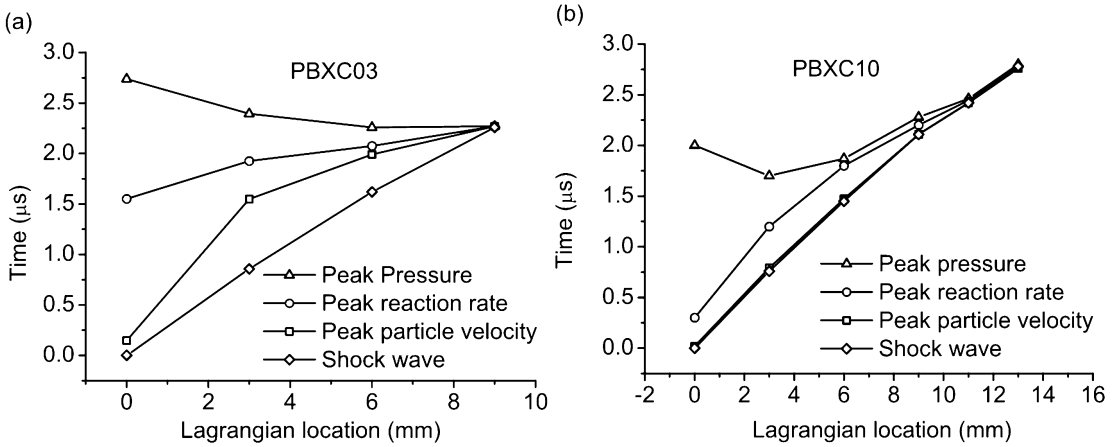

Figure 11. Comparison of trajectories of the initial shock wave, the peak particle velocity, the peak reaction rate and the peak pressure.

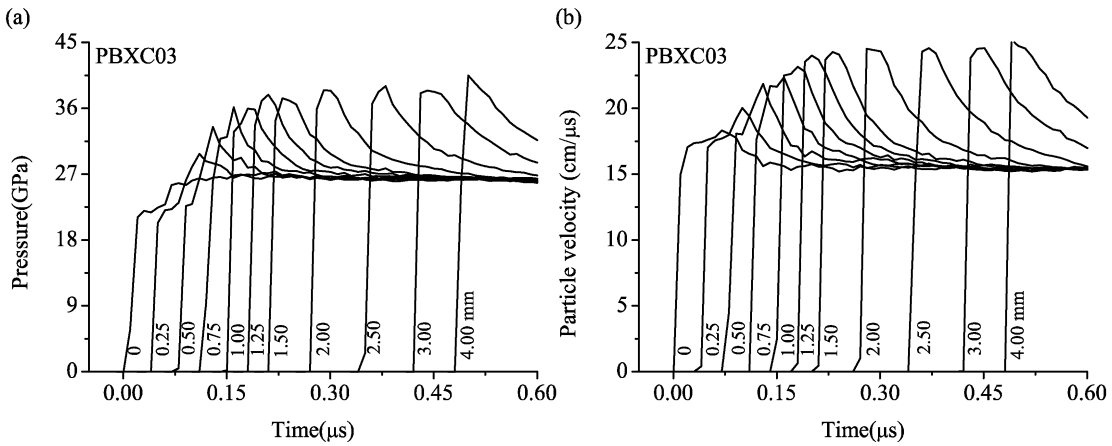

Figure 12. Pressure-time histories and particle velocity-time histories iCn PBXC03 via the aluminum flyer impact at the speed of 2800 m/s.

PBXC10, respectively. It is found that the peak reaction rate occurs later than the peak particle velocity and earlier than the peak pressure. Moreover, with the increasing of the Lagrangian location, the particles of detonation products are accelerated by stronger compression waves, and the peak reaction rate is also close to the precursory shock-wave front.

The above-mentioned results are the detonation growth processes of PBXC03 and PBXC10 under each critical initiation pressure loading, and it is found that the detonation growth characteristic of PBXC03 at lower loading pressure obviously differs from that of the insensitive PBXC10. Then, whether the PBXC03 will show similar detonation growth characteristics with that of the insensitive PBXC10 if the loading pressure is increased? To answer this question, an aluminum flyer with the thickness of 10 mm impacting experiment on PBXC03 at the speed of 2800 m/s is performed. The pressure-time histories and the particle velocity-time histories are shown in Figure 12. It is found, under the action of a high impact load, that the detonation growth zone narrows down and the chemical reaction occurs more closely to the precursory shock-wave front. However, there is no essential change in the characteristics of the detonation growth in PBXC03, which still present the pressure-increasing behind the precursory shock wave and the peak pressure keeps in chasing up the precursory shock wave front. Thus, the main driving force for the pressure-increasing behind the precursory shock-wave front in PBXC03 is the compression wave resulted from the rapid combustion reaction.

5 Conclusions

Based on the experimental data of in-situ pressure-time histories in PBXC03 and PBXC10 and the corresponding numerical results, a new multi-component DZK reaction rate model is developed. Some conclusions are drawn out as follows:

(1) Once the parameters in the DZK reaction rate model for each explosive component are determined, the multi-component DZK reaction rate model can be used directly to predict well the shock initiation characteristics of multi-component PBXs with any explosive component proportion.
(2) Pressure-time histories of PBXC03 shows as a shape of hump, while that of PBXC10 shows as a step increase during the whole shock initiation process.
(3) The shock initiation behavior of the HMX-based PBX is mainly controlled by the density of hot spots and shows the accelerated reaction characteristics, and that of the TATB-based PBX is basically determined by the combustion reaction process, which featured by a stable reaction characteristic. This finding is consistent with the conclusion of K.F. Grebenkin [12].

Acknowledgements

This work was supported by the NSAF Joint Fund (Grants No. U1630113) and the Innovative Group of Material and Structure Impact Dynamics (Grants No. 11521062).

References

[1] O. Bolton, L. R. Simke, P. F. Pagoria, A. J. Matzger, High power explosive with good sensitivity: a 2:1 cocrystal of CL-20: HMX, *Cryst. Growth Des.* **2012**, *12*, 4311–4314.
[2] C. M. Tarver, T. D. Tran, Thermal decomposition models for HMX-based plastic bonded explosives, *Combust. Flame.* **2014**, *137*, 50–62.
[3] J. J. Xiao, W. R. Wang, J. Chen, G. F. Ji, W. Zhu, H. M. Xiao, Study on structure, sensitivity and mechanical properties of HMX and HMX-based PBXs with molecular dynamics simulation, *Comput. Theor. Chem.* **2012**, *999*, 21–27.
[4] R. L. Gustavsen, S. A. Sheffield, R. R. Alcon, J. W. Forbes, C. M. Tarver, F. Garcia, Embedded electromagnetic gauge measurements and modeling of shock initiation in the TATB based explosives LX-17 and PBX 9502, *Shock Compression of Condensed Matter*, Atlanta, GA, 24–29 June, **2001**, 1019–1022.
[5] P. A. Urtiew, J. W. Forbes, F. Garcia, C. M. Tarver. Shock initiation of UF-TATB at 250 °C. *Shock Compression of Condensed Matter*, Atlanta, GA, 24–29 June, **2001**, 1039–1042.
[6] M. B. Talawar, A. P. Agarwal, M. Anniyappan, G. M. Gore, S. N. Asthana, S. Venugopalan, Method for preparation of fine TATB (2–5 microm) and its evaluation in plastic bonded explosive (PBX) formulations, *J. Hazard. Mater.* **2006**, *137*, 1848–1852.
[7] L. J. Wen, *Research on mesoscopic reaction rate model of shock initiation of PBX*, Beijing Institute of Technology, Beijing **2011**. (In chinese).
[8] L. J. Wen, Z. P. Duan, L. S. Zhang, Z. Y. Zhang, Z. C. Ou, F. L. Huang, Effects of HMX particle size on the shock initiation of PBXC03 explosive, *Int. J. Nonlin. Sci. Num. Simul.* **2012**, *13*, 189–194.
[9] C. Wang, L. Chen, J. Y. Wu, Q. Liu, X. M. Hu, Shock to initiation characters of heated explosives with different confinement, *Propell. Explos. Pyrot.* **2016**, *41*, 383–392.
[10] J. Sun, H. Huang, Y. Zhang, M. X. Zheng, J. L. Liu, In-stiu coating of TATB on HMX, *Chin. J. Energ. Mater.* **2006**, *14*, 330–332.
[11] C. Wei, H. Huang, X. Duan, C. Pei, Structures and properties prediction of HMX/TATB co-crystal, *Propell. Explos. Pyrot.* **2011**, *36*, 416–423.
[12] K. F. Grebenkin, Comparative analysis of physical mechanisms of detonation initiation in HMX and in a low-sensitive explosive (TATB), *Combust. Explos. Shock Waves* **2009**, *45*, 78–87.
[13] R. Austin, N. Barton, W. Howard, L. Fried. Modeling pore collapse and chemical reactions in shock-loaded HMX crystals. *Shock Compression of Condensed Matter*, Seattle, WA, 7–12 July, **2013**, 500, 052002.
[14] M. Ozlem, D. W. Schwendeman, A. K. Kapila, W. D. Henshaw, A numerical study of shock-induced cavity collapse, *Shock Waves* **2012**, *22*, 89–117.
[15] K. Kim. Development of a model of reaction rates in shocked multicomponent explosives. *Proceeding of the 9th symposium (International) on Detonation*, Portland, OR, 28 August 28–1 September, **1989**, 593–603.
[16] J. Massoni, R. Saurel, G. Baudin, G. Demol, A mechanistic model for shock initiation of solid explosives, *Phys. Fluids* **1999**, *11*, 710–736.
[17] T. M. Willey, T. V. Buuren, J. R. I. Lee, G. E. Overturf, J. H. Kinney, J. Handly, B. L. Weeks, J. Ilavsky, Changes in pore size distribution upon thermal cycling of TATB-based explosives measured by ultra-small angle X-ray scattering, *Propell. Explos. Pyrot.* **2010**, *31*, 466–471.
[18] C. M. Tarver, M. R. Manaa, Chemistry of detonation waves in condensed phase explosives, *Cheminform* **2006**, 37.
[19] A. Kapahi, Dynamics of void collapse in shocked energetic materials: physics of void-void interactions, *Shock Waves* **2013**, *23*, 537–558.
[20] L. Tran, H. S. Udaykumar, Simulation of void collapse in an energetic material, part 1: inert case, *J. Propul. Power* **2006**, *22*, 947–958.
[21] L. Tran, H. S. Udaykumar, Simulation of void collapse in an energetic material, part 2: reactive Case, *J. Propul. Power* **2006**, *22*, 959–974.
[22] T. T. Zhou, J. F. Lou, Y. G. Zhang, H. J. Song, F. L. Huang, Hot spot formation and chemical reaction initiation in shocked HMX crystals with nanovoids: a large-scale reactive molecular dynamics study, *Phys. Chem. Chem. Phys.* **2016**, *18*, 17627–17645.
[23] A. Kapahi, H. S. Udaykumar, Three-dimensional simulations of dynamics of void collapse in energetic materials, *Shock Waves* **2015**, *25*, 177–187.
[24] N. K. Rai, M. J. Schmidt, H. S. Udaykumar, High-resolution simulations of cylindrical void collapse in energetic materials: effect of primary and secondary collapse on initiation thresholds, *Phys. Rev. Fluids* **2017**, 2.
[25] P. C. Souers, R. Garza, P. Vitello, Ignition & growth and JWL++ detonation models in coarse zones, *Propell. Explos. Pyrot.* **2002**, *27*, 62–71.
[26] J. Starkenberg. Modeling detonation propagation and failure using explosive initiation models in a conventional hydrocode. *Proceeding of the 12th Symposium (International) on Detonation*, San Diego, CA(US), 11–16 August, **2002**.
[27] J. Starkenberg, T. M. Dorsey. An assessment of the performance of the history variable reactive burn explosive initiation model in the CTH code. *Proceeding of the 11th Symposium (International) on Detonation*, Snowmass, CO, August 30–September 4, **1998**, 621–631.
[28] M. S. Shaw, R. Menikoff. A reactive burn model for shock initiation in a PBX: scaling and separability based on the hot spot

concept. *Proceeding of the 14th Symposium (International) on Detonation*, Coeur d' alene, Idaho, 11–16 April, **2010**.

[29] S. G. Cochran, *Statistical treatment of heterogeneous chemical reaction in shock-initiated explosives*, Report UCID-18548, Lawrence Livermore National Laboratory, Livermore, CA (United States), **1980**.

[30] L. G. Hill, B. Zimmermann, A. L. Nichols, On the burn topology of hot-spot reactions. *AIP Conf. Proc.* **2009**, *1195*, 432–435.

[31] A. L. Nichols, C. M. Tarver. A statistical hot spot reactive flow model for shock initiation and detonation of solid high explosives. *Proceeding of the 12th Symposium (International) on Detonation*, San Diego, CA (US), 11–16 August, **2002**.

[32] Z. P. Duan, L. J. Wen, Y. R. Liu, Z. C. Ou, F. L. Huang, Z. Y. Zhang, A pore collapse model for hot-spot ignition in shocked multi-component explosives, *Int. J. Nonlin. Sci. Num. Simul.* **2010**, *11*, 19–24.

[33] Y. R. Liu, Z. P. Duan, Z. Y. Zhang, Z. C. Ou, F. L. Huang, A mesoscopic reaction rate model for shock initiation of multi-component PBX explosives, *J. Hazard. Mater.* **2016**, *317*, 44–51.

[34] B. M. Dobratz, LLNL Explosives Handbook Properties of Chemical Explosives and Explosive Simulants, Report No. UCRL-52997, **1981**.

[35] P. A. Urtiew, K. S. Vandersall, C. M. Tarver, F. Garcia, *Initiation of heated PBX-9501 explosive when exposed to dynamic loading*, Report UCRL-CONF-214667, Lawrence Livermore National Laboratory, Livermore, CA (United States), **2005**.

[36] P. A. Urtiew, C. M. Tarver, Shock initiation of energetic materials at different initial temperatures (review), *Combust. Explos. Shock Waves* **2005**, *41*, 766–776.

[37] B. A. Khasainov, B. S. Ermolaev, H. N. Presles, P. Vidal. On the effect of grain size on shock sensitivity of heterogeneous high explosives. *Shock Wave* **1997**, *7*, 89–105.

[38] H. Moulard, J. W. Kury, A. Delclos, The effect of RDX particle size on the shock sensitivity of cast PBX formulations, *Proceeding of the 8th Symposium (International) on Detonation*, Albuquerque, NM, **1985**, 1, 248–257.

[39] R. R. Bernecker, R. L. Simpson, Further observations on HMX particle size and buildup to detonation. *AIP Conf. Proc.* **1998**, *429*, 719–722.

[40] S. R Li, Z. P. Duan, L. J. Wen, Z. L. Bai, Z. C. Ou, F. L. Huang, Mesoscopic effects on shock initiation of multi-component plastic bonded explosives, *J. Appl. Phys.* **2018**, *124*, 045903.

Manuscript received: December 29, 2018
Revised manuscript received: March 10, 2019
Version of record online: April 17, 2019

